6th International Biennial Conference on UltraFine Grained and NanoStructured Materials
UF6NSM2017 12-13 November 2017
International Convention Center, Kish Island, Iran
UNIVERSITY OF TEHRAN UNIVERSITY OF TRENTO KISH FREE ZONE

Investigation the effect of anodization voltage on the geometrical properties and photocatalytic activity of TiO2 nanotube arrays for degradation of p-nitrophenol

Kamyar Khoshsirat Janekbari [1, a)], Neda Gilani [1, b)], Azadeh Ebrahimian Pirbazari [1, c)]

[1] *Fouman Faculty of Engineering, College of Engineering, University of Tehran, P. O. Box 43515-1155, Fouman 43516-66456, Iran,*

[a)] k.khoshsirat@ut.ac.ir
[b)]Corresponding author: gilani@ut.ac.ir
[c)] aebrahimian@ut.ac.ir

Abstract. *p*-nitrophenol (PNP) is a nitroaromatic compound that poses a potential environmental hazard because of its acute toxicity, high carcinogenicity, low biodegradability and cumulative effect. Titanium dioxide (TiO_2) nanotubes have shown great potential as ideal and powerful photocatalysts in purification of polluted water due to their high photo oxidation, anti-fogging, nontoxicity, good chemical stability and low cost. Therefore, TiO_2 nanotube arrays were fabricated by two-step anodization process at 30,40 and 50V; and were used in photocatalytic degradation of organic pollution *p*-nitrophenol. In order to have the crystal structure, nanotubes were annealed at 450 °C for 2 hours. Characterizing of TiO_2 nanotubes were evaluated by FESEM, XRD and Spectrophotometry analyses. Effect of anodization voltage on nanotube's length and diameter were investigated. The result showed that as anodization voltage increases from 30V to 50V, nanotube's length, diameter and wall thickness increase linearly from 1.4 µm to 4.8 µm, 45 nm to 100nm and 15nm to 25 nm, respectively. Increasing in anodization voltage lead to enhancement in porosity (0.4-0.5) and roughness factor (109-194) of TiO_2 nanotubes, respectively. By investigating kinetic of degradation of *p*-nitrophenol, it was observed that mechanism of photocatalytic degradation for all samples are followed first order kinetic. The results indicate that amongst all synthesized samples, 50 V sample with 38%, shows the most efficiency in degradation of *p*-nitrophenol under UV irradiation.

Keywords: TiO_2 nanotubes, Photocatalytic Degradation, *p*-nitrophenol, Anodization Voltage

INTRODUCTION

An even-increasing discharge of biorefactory organic compounds into the environment has caused serious problems in water and wastewater treatment because these compounds cannot be degraded effectively by traditional technologies. Advanced oxidation processes (AOPs) are presently attractive for such biorefactory wastewater treatment either as a pretreatment or mineralization process by generation of highly powerful oxidant of hydroxyl radical in situ [1]. Among the AOPs, photocatalytic degradation has emerged as a versatile technique for the removal of pollutants from water because of its desirable properties such as low cost, high efficiency, complete mineralization of various organic compounds, and no secondary pollution [2]. P-nitrophenol (PNP) is a nitro aromatic compound that poses a potential environmental hazard because of its acute toxicity, high carcinogenicity, low biodegradability and

cumulative effect, and has been listed as a priority pollutant by the United States Environmental Protection Agency. Nitro aromatic compounds are widely used as intermediates in the preparation of coal chemicals, petrochemicals, dyes and explosives, which may cause a reduction in the transfer of atmospheric oxygen to water and consequently a rapid reduction in the water biomass because of the insoluble liquid phase floating on the water surface [3]. Titanium dioxide (TiO_2) has been shown to be superior to other photocatalysts such as ZnO, WO, and CdS due to its high chemical stability, non-toxicity and large band gap (Eg =3.20). However, the photocatalytic efficiency of TiO_2 appears to be somewhat limited by its high degree of electron-hole recombination, wide band-gap, conspicuous settlement and limited adsorption capability for pollutants [4]. TiO_2 nanotube arrays not only have the advantages of traditional TiO_2 including high catalytic activity, nontoxicity, and long-term photostability, but also offer a large surface area, excellent dielectric properties, and strong adsorption capacity [5]. Moreover, high recovery efficiency is another advantages for multiple usage of TiO_2 nanotubes in photocatalytic degradation. among the TiO_2 nanotubes fabrication methods, anodic oxidation technique because of controllable parameter and producing highly ordered array structures, has been extensively investigated.

Our surveys have shown that most of researches on photocatalytic degradation of *p*-nitrophenol are using TiO2 nanoparticles [6-8]. Some papers have investigated photocatalytic degradation *p*-nitrophenol are using modified TiO2 nanotubes [9,10]. In this paper, we investigate the effect of anodization voltage on geometry of TiO2 nanotubes arrays fabricated by anodization process and effect of these parameters on photocatalytic activity of TiO2 nanotubes for degradation of *p*-nitrophenol.

EXPERIMENTS

Fabrication of TiO2 Nanotubes Arrays

Commercial titanium foils (with 97% purity, 0.25 mm in thickness) were cut into pieces of 3 by 9 cm. First of all, for degreasing, sheets were immersed in acetone, ethanol and deionized water for about 10 min, respectively. To obtain a completely smooth and sleek surface, chemical polishing in a mixture of HF, HNO3 and deionized water solution with a volume ratio 1:4:5 was used. For Anodizing, titanium sheets were used for both the anode and the cathode. The first step was performed in an ethylene glycol based electrolyte containing 2 vol % deionized water and 0.5 wt% ammonium fluoride at a constant voltage of 30, 40 and 50 V at room temperature for 1.5 h. Then, the resulting TiO2 nanotubes from the first step were removed by acid treating process using HF and deionized water solution. To achieve the orderly and aligned TiO2 nanotubes, the second step of anodizing was done in the same condition as the first step for 6 h. Subsequently, to obtain a crystalline structure, the temperature of the TiO2 nanotubes was raised to 450 °C at a rate of 3 °C/min. They were kept at that temperature for 2 h. The synthesized samples are referred to as NT-(x) in which x refers to the anodization voltage.

Structure and Morphology Characterization

The surface morphology, length and diameter of the prepared nanotubes were first examined using the field-emission scanning electron microscopy (FESEM; MIRA3 TESCAN, Czech Republic). In order to determine the crystal structure of the annealed titanium dioxide nanotubes, X-ray diffraction (XRD; Philips PW1840) measurement with Cu K α radiation was used.

Photocatalytic Degradation of *p*-nitrophenol

In all experiments, 100 ml of *p*-nitrophenol solution with an initial concentration of 20 ppm were used. Photocatalytic degradation was performed by using 3cm×3cm sheet of the prepared catalysts at different voltages under UV radiation (400 W, Kr lamp Osram, Germany) for 4 hours. Prior to starting the irradiation, the methylene blue solution and the catalysts were magnetically stirred in the dark for ten minutes until absorption and desorption reached equilibrium. Changes in the concentration of *p*-nitrophenol during the photocatalytic degradation process

were measured by changes in the methylene blue absorption spectrum at 318 nm wavelength obtained from UV–Vis spectrophotometer device (Rayleigh, UV-2601 UV–VIS, China).

RESULT AND DISCUSSION

FESEM Analysis

In Fig. 1, the surface and cross section field-emission scanning electron microscopy images (FESEM) of the titanium dioxide nanotubes are observed. Fig. 1(A)–(C) show the images of the TiO2 nanotubes surface fabricated at voltages of 30, 40 and 50 V. According to Fig. 1(A)–(C), it can be seen that the TiO2 nanotubes have regular and honeycomb surface structures because of fluorine ions in electrolyte solution. Cross sectional images of the TiO2 nanotubes are observed in Fig. 1(D)–(F). These figures indicate that by removing the nanotubes grown in the first-step anodization, many ordered hexagonal imprint patterns are left on Ti substrates, greatly improving the uniformity and orderliness of the TiO2 nanotubes during the second-step anodization. With the help of FESEM images shown in Fig. 1, length, diameter and the length to diameter ratio of the prepared TiO2 nanotubes at constant voltages of 30, 40 and 50 V, presented in Table 1, are obtained. The results presented in Table 1 show that due to an increase in the voltage from 30 to 50 V, the diameters of the nanotubes increase from 45 to 100 nm. This increase is due to applying a greater electric field that leads to more surface etching [11]. The results presented in Table 1 also indicate that the lengths of the nanotubes increase as the anodization voltage increases. The reason for this increase is the increase of the oxidation reactions and oxide layer dissolution [12]. According to Table 1, when the anodization voltage increases from 30 to 50V, the nanotubes' length growth from 1.4 μm to 4.8 μm and the nanotubes' diameter increases linearly from 45 nm to 100nm with rate of are obtained 2.73 nm/V. Among the geometric parameters, the of the TiO2 nanotubes, defined as the ratio of surface area occupied by pores to the whole surface area, can be determined from Eqs. (1) [13].

$$p = 1 - \frac{2\pi w(w+d)}{\sqrt{3}(d+2w)^2} \tag{1}$$

where P, d, and w are the respective porosity, pore diameter and wall thickness of the TiO2 nanotubes. Based on the corresponding size parameters derived from the FESEM analysis in Table 1 and Eqs. (1), the porosity is calculated and presented in Table 2. According to Table 2, it is observed that the anodization voltage significantly affects the porosity as geometrical parameters. A decrease in the anodization voltage from 30 to 50 V, leads to decreased porosity of the TiO2 nanotubes.

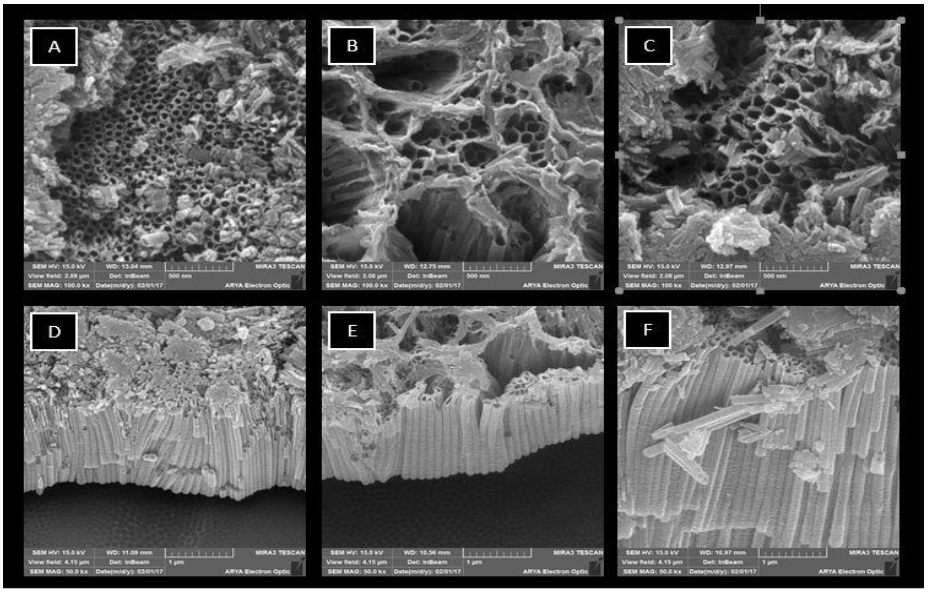

FIGURE 1. FESEM images from surface of the (A) NT-30, (B) NT-40, (C) NT-50, cross section of the (D) NT-30, (E) NT-40, (F) NT-50

TABLE 1. The geometrical properties of the synthesized TiO2 nanotubes calculated by FESEM

Samples	Anodization Voltage (V)	Average Nanotube Length (µm)	Average Nanotube Diameter (nm)	Average Nanotube Wall thickness (nm)
NT-30	30	1.4	45	15
NT-40	40	1.8	70	21
NT-50	50	4.6	100	25

TABLE 2. Porosity of the synthesized TiO2 nanotubes

Samples	Porosity
NT-30	0.4169
NT-40	0.4474
NT-50	0.4962

X-ray Diffraction Analysis

Regarding the structure of TiO2, there are three crystalline phases in titanium dioxide, namely the anatase, rutile, and brookite phases, which among them, the anatase phase has a higher photocatalytic property than the other two due to its high refraction index and low extinction coefficient [14]. Fig. 2 represents the XRD patterns of the synthesized

samples which were calcinated at 450 °C for 2 h after their fabrication. The diffraction peaks at 2θ of 25.5°, 37.3°, 38.1°, 48.2°, 54.2° and 55.2° which are equivalent to the Miller indexes (101), (103), (004), (200), (105) and (211) can be indexed to the characteristic peaks of anatase phase after calcination at the temperature of 450 °C [15].

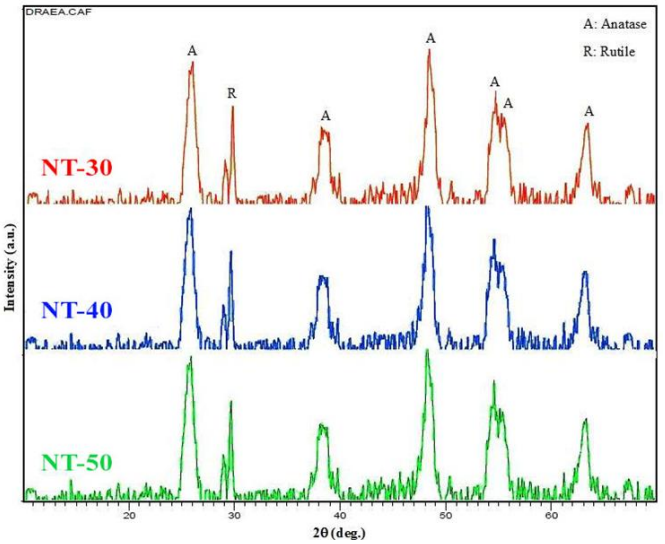

FIGURE 2. XRD patterns of the TiO2 nanotube arrays calcinated at 450 °C.

The Results of *p*-nitrophenol Photocatalytic Degradation

Fig. 3 shows the percentage of the degradation of *p*-nitrophenol versus irradiation time which is calculated using Eq. (2) [16].

$$X_{PNP} = \frac{C_0 - C}{C} \times 100 \quad (2)$$

Where X_{PNP} is the percentage of the degradation of *p*-nitrophenol, C is the concentration of *p*-nitrophenol and C_0 is the initial concentration of *p*-nitrophenol. According to Fig. 3, it can be seen that an increase in the voltage from 30 to 50 V caused the percentage of the photocatalytic degradation of *p*-nitrophenol to increase from 27% to 38% under irradiation for 240 min. n Fig. 3 (a), it can also be observed that little absorption is done in the 30 minutes before the start of the UV radiation (zero time). Thus it can be concluded that the TiO2 nanotubes, in addition to creating unstable hydroxyl radicals and superoxide ions in water for the degradation of *p*-nitrophenol, can also degrade *p*-nitrophenol by absorbing it on their surface after irradiation by their photon activated surface.

According to the Langmuir-Hinshelwood mechanism, the differential Equation of the concentration changes versus time follows Eq. (3) [17].

$$r = -\frac{dC}{dt} = \frac{kKC}{1 + KC} \quad (3)$$

where C is the concentration of *p*-nitrophenol (ppm), k is the rate constant (min^{-1}), K is the adsorption constant and t is the degradation time (min). For the low initial concentrations of *p*-nitrophenol, the term KC in the denominator can be neglected because it is very small with respect to 1. Therefore, Eq. (3) can be written as follows:

$$r = -\frac{dC}{dt} = kKC = k_{app}t \quad (4)$$

Where k_{app} is the apparent rate constant. After the integration of the both sides of Eq. (4), Eq. (5) which represents the first order kinetics is obtained:

$$\ln\left(\frac{C}{C_0}\right) = -k_{app}t \tag{5}$$

Where C_0 is the initial concentration of *p*-nitrophenol and is equal to 20 ppm. In Fig. 3 (b), the graph of $\mathrm{Ln}(C/C_0)$ versus the degradation time of *p*-nitrophenol is plotted for the three samples of NT-30, NT-40 and NT-50. In this graph, the irradiation begins from the zero time and before this time, the graph is related to the presence of the catalyst in the pollutant solution in the dark. According to Fig. 3 (b), it can be seen that the changes of $\mathrm{Ln}(C/C_0)$ versus time are linear for all samples. So the kinetics of the degradation of *p*-nitrophenol follows first order kinetics.

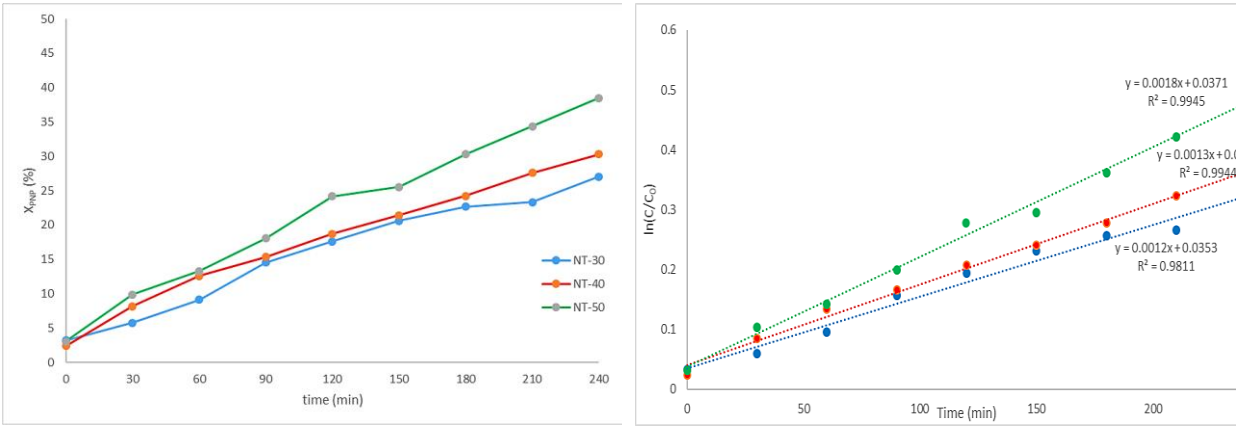

(a) (b)

FIGURE 3. (a) Photocatalytic degradation of *p*-nitrophenol by the synthesized samples under UV irradiation and (b) Photocatalytic degradation kinetics of *p*-nitrophenol by the synthesized samples

CONCLUSION

Highly ordered TiO2 nanotubes were fabricated by two-step anodization process in various voltage of 30,40 and 50V in order to photocatalytic degradation of *p*-nitrophenol. Anatase crystalline phase was obtained by annealing the TiO2 nanotubes at 450 °C. In order to investigate the effect of the TiO2 nanotubes' diameter and length on the photocatalytic degradation of *p*-nitrophenol, the TiO2 nanotubes were fabricated at three anodization voltages of 30, 40 and 50 V. The results showed that an increase in the anodization voltage caused an increase in the nanotubes' diameter and length from 1.4 μm to 4.8 μm, 45 nm to 100nm and 15nm to 25 nm, respectively. The results showed that a decrease in the voltage leads to decreased porosity. Furthermore, as a result of the decrease in the anodization voltage, the photocatalytic activity of the TiO2 nanotubes increases. In this research, the best photocatalytic degradation was of the sample that was fabricated at 50 V which while having the highest porosity (0.4962) had the best apparent rate constant (0.0018 min^{-1}) and the highest degradation of *p*-nitrophenol (38%) in comparison to the other samples.

ACKNOWLEDGMENTS

The authors would like to acknowledge the College of Engineering, University of Tehran for their esteemed financial support.

REFERENCES

1. M. Zhou and L. Lei, Chemosphere **63** (6), 1032-1040 (2006).

2. J. Lv, H. Gao, H. Wang, X. Lu, G. Xu, D. Wang, Z. Chen, X. Zhang, Z. Zheng and Y. Wu, Applied Surface Science **351**, 225-231 (2015).
3. L. Li, Y. Feng, Y. Liu, B. Wei, J. Guo, W. Jiao, Z. Zhang and Q. Zhang, Applied Surface Science **363**, 627-635 (2016).
4. S.-J. C. Shun-Xing Li, Feng-Ying Zheng, Dyes and Pigments 92 (2), 188-193 (2012).
5. X. Zhang, J. Zhou, Y. Gu and D. Fan, Journal of Nanomaterials 16 (1), 42 (2015).
6. S.-x. Li, F.-y. Zheng, X.-l. Liu, F. Wu, N.-s. Deng and J.-h. Yang, Chemosphere 61 (4), 589-594 (2005).
7. R. Rahimi, S. S. Moghaddam and M. Rabbani, Journal of sol-gel science and technology **64** (1), 17-26 (2012).
8. J. Lea and A. A. Adesina, Journal of Chemical Technology and Biotechnology 76 (8), 803-810 (2001).
9. L. Yang, S. Luo, Y. Li, Y. Xiao, Q. Kang and Q. Cai, Environmental Science & Technology 44 (19), 7641-7646 (2010).
10. H. Feng, T. Tran. T, L. Chen, L. Yuan and Q. Cai, Chemical Engineering Journal 215, 591-599 (2013).
11. T. Noeiaghaei, J.-H. Yun, S. W. Nam, K. D. Zoh, V. G. Gomes, J. O. Kim and S. R. Chae, Water Science and Technology 71 (9), 1301-1309 (2015).
12. Y. L. Pang, S. Lim, H. C. Ong and W. T. Chong, Applied Catalysis A: General 481, 127-142 (2014).
13. N. Vaenas, T. Stergiopoulos, A. G. Kontos, V. Likodimos and P. Falaras, Electrochimica Acta 113, 490-496 (2013).
14. G.-j. Cao, B. Cui, W.-q. Wang, G.-z. Tang, Y.-c. Feng and L.-p. Wang, Transactions of Nonferrous Metals Society of China **24** (8), 2581-2587 (2014).
15. Ratnawati, J. Gunlazuardi, E. L. Dewi and Slamet, International Journal of Hydrogen Energy **39** (30), 16927-16935 (2014).
16. M. Dimitrov, R. Ivanova, N. Velinov, J. Henych, M. Slušná, V. Štengl, J. Tolasz, I. Mitov and T. Tsoncheva, Nano-Structures & Nano-Objects **7**, 56-63 (2016).
17. L. Qin, Q. Chen, R. Lan, R. Jiang, X. Quan, B. Xu, F. Zhang and Y. Jia, Journal of Materials Science & Technology **31** (10), 1059-1064 (2015).